Integrated AC electrokinetic cell separation in a closed-loop device†

Zachary Gagnon, Jill Mazur and Hsueh-Chia Chang*

Received 20th August 2009, Accepted 11th November 2009
First published as an Advance Article on the web 4th January 2010
DOI: 10.1039/b917220c

We integrate electrothermally induced micro-pumps and dielectrophoretic (DEP) traps into micro-circulating fluidic channel loops for yeast cell concentration and separation, two important on-chip cell manipulation tasks, with the same embedded electrodes on-chip. Each fluidic loop design contains well-defined high and low field regions that serve for both fluid transport and cellular manipulation. From a detailed study into the frequency dependent DEP behavior of viable (live) and non-viable (dead) yeast, we demonstrate several operating modes that utilize positive DEP (pDEP) and negative DEP (nDEP) to concentrate both types of cells at either the high or low electric field region and to separate one cell type to a high-field region and one to a low-field region. Because the cells visit the trapping regions repeatedly with the circulating loop design and because of the high shear rates at these stations, our device offers very rapid cell separation and concentration. Two circulating loop designs – one a four-sided square loop, the other a three-sided triangle, with different spatial symmetries and with linear dimensions less than 1 mm, are presented.

1.0 Introduction

The precise movement and relocation of fluid and bioparticles within a confined microchannel network is an essential requirement for any lab-on-a-chip (LoC) type device. Research towards this goal has resulted in an array of microfluidic pumps, valves, mixers, and cell sorters, all aimed at specific micro-manipulation tasks.[1–3] Of course the hallmark of this field is to essentially integrate and automate these units into a fully-functional device for automated fluid handling.

AC electrokinetic phenomena such as dielectrophoresis (DEP), AC electro-osmosis (ACEO) and electrothermal (ET) effects are quickly becoming popular manipulation tools for LoC and microfluidic devices.[4] The use of non-uniform AC fields to drive interfacial polarization at the surface of cells, colloids and fabricated microelectrodes ultimately leads to the formation of bulk fluid flow (ACEO, ET) and particle motion (DEP). By controlling the applied field magnitude and frequency, finely controlled pumping and cell-specific bioparticle manipulation becomes feasible.[5–10] The AC electric field is generated with microfabricated planar electrodes in contact with aqueous solution. Due to the small micron-sized separation length of the electrodes, large electric field strengths (10 kV m^{-1}) can be generated with only a few applied volts. Additionally, the driving high frequency field prevents bubble generating Faradaic reactions from occurring and allows the electrodes to be fabricated directly within the channel.[11]

The purpose of this article is to demonstrate the potential of AC electrokinetic devices for automated on-chip bioparticle processing. ET micro-pumps and DEP traps are integrated into insulating polymeric PDMS microchannels. In this manner, the two phenomena complement each other – bioparticles are electrothermally convected over DEP traps where they are selectively separated from suspension. By tailor designing the microelectrode geometry, the AC field penetration depth, channel height, and active electrode configuration we demonstrate the ability to selectively trap and separate viable and non-viable yeast cells at specific DEP trap locations. Without deactivating the device, these active trapping zones can be relocated to different parts of the microchannel with a simple positional adjustment to the active electrode. Using the same electrode geometry the device can be converted from a bulk non-selective cell trap to a cell specific trap with a simple increase or decrease in channel height.

There have been many studies utilizing AC electrokinetic forces, specifically DEP, for the cell separations. Initial experiments were done batch-wise, where small volumes of cellular suspension were added to the surface of a fabricated electrode array.[12–15] The applied electric field frequency, voltage and electrolyte composition were then adjusted and the resulting effects on cell separation and DEP mobility was studied. There has been work characterizing the electric field effect on cell clustering,[14] the effect zwitterion buffers have on cell levitation[13] and the use of castellated electrode structures for batch-wise viable and non-viable yeast cell separation by DEP.[12]

More recently, however, microfluidic channels have become integrated with DEP electrode structures and resulted in the development of more complex cell processing and cell separation. Typically, such cell processing is done in a linear flow format where an array of addressable DEP traps are integrated into a microchannel several millimetres in length.[16–19] In this manner, a cell suspension is introduced into the channel and through interaction with the DEP traps integrated along the channel surface, a specific cell species is separated from the incoming fluid flow. In this work we seek to reduce the number of

Center for Microfluidics and Medical Diagnostics, Department of Chemical and Biomolecular Engineering, University of Notre Dame, Notre Dame, Indiana, 46556, USA. E-mail: hchang@nd.edu; Fax: +574-631-8366; Tel: +574-631-9185

† Electronic supplementary information (ESI) available: Supplementary video. See DOI: 10.1039/b917220c

required DEP traps for cell separation by continuously circulating a cell suspension repeatedly over the same DEP traps and introducing integrated electrokinetic components that serve as both fluid pumps and cellular DEP traps.

The AC electrokinetic components allow our device to deviate from the conventional linear-flow format in which the sample visits each trapping station on the chip only once. High-throughput sorting often requires numerous sorting stations, which translates into a large chip with long residence time due to the high linear fluid velocity.[18] We increase the residence time of the sample within the chip not with a longer channel but with a circular-loop design that is becomes possible with the AC electrokinetic components. In conventional pressure-driven flow with mechanical components, a circular fluid or particle flux cannot be achieved without valving, as the continuous pressure field in the fluid must necessarily be periodic around the circuit and hence cannot offer a pressure gradient that is always in the same direction along the circuit.[20] With AC pumping and DEP, the forces are imparted locally along the loop and a circulating flow can be achieved. With this loop design, the sample visits each DEP separation or concentrating component repeatedly with each circulating pass, considerably reducing the number of components necessary and the size of the chip. As in the classical engineering recycling design, we offer side streams to feed new samples or "bleed off" concentrated product streams. The particles can remain within the small chip for hours and yet still experience strong hydrodynamic shear imparted by the circulating flow – a feature that should prove useful for the study of long-term cell response to hydrodynamic shear. We demonstrate the capabilities and potentials of the integrated AC electrokinetic components here with simple chips that can eventually be scaled up into highly complex and automated bioparticle processing units.

2.0 Electrokinetic phenomena

Electrokinetic manipulation is made possible by the unique field induced interfacial polarization that results when an electrolyte is placed in contact with a pair of micro-electrodes and confined to a relatively small (<1mm) length scale. Charging the electrodes with an externally applied AC potential can induce an electric field in solution and attract counter-ions to both the electrode and any suspending bioparticle surface. This induced accumulation of ions forms a very thin (<1 μm) capacitor-like charged region known as the electrical double layer (EDL) on the particle or electrode surface. The same field that charges the particle and electrode can exert a force on the induced charge leading to a net motion of both the bioparticle and the fluid. The terms describing these forces are dielectrophoresis and electro-osmosis, respectively. We discuss the individual characteristics of such phenomena in relation to micro-pumping and cellular manipulation below.

2.1 Micro-pumping with AC electro-osmosis

AC electro-osmostic (ACEO) fluid flow is a popular non-mechanical technique for fluid mixing and transport. In the past decade, a variety of ACEO micro-pumps have emerged.[8,9] The basic design consists of a pair of micro-electrodes in contact with an electrolyte solution. A high frequency (0.1–1 MHz) AC field is dropped across the electrodes to produce an AC electric field in solution, charging the EDL on the electrode surface much like a capacitor. The accumulation of charge must partially, but not entirely, screen the external electric field such that there is still a tangential component of the electric field acting on each electrode EDL to generate flow. Because it takes a finite amount of time for the EDL to charge, ACEO flow has a distinct maximum in observed flow velocity at a characteristic relaxation (inverse RC) time scale for the electrode-electrolyte circuit. This characteristic charging frequency, ($D/\lambda l$), where D is the ion diffusivity, λ is the Debye layer thickness and l the electrode separation, for most conditions occurs between 100 and 500 kHz.[19]

While ACEO fluid transport is possible, the driving body force behind this is limited to within the thin (~100 nm) EDL on the electrode surface. In fact, ACEO flow is negligible at high buffer conductivities where the double layer is exceedingly thin. Therefore, ACEO flow, while effective, is highly inefficient and often suffers from a maximum fluid velocity typically on the order of 100 μm s^{-1}.[9] In this work, we seek a more attractive alternative to ACEO flow. Below, we introduce a rather newly observed flow phenomena driven by both double layer charging and temperature generating Joule heating to drive a much stronger (up to 6.5 mm s^{-1}) and longer range micro-pump.[10]

2.2 Electrothermal flow

Unlike ACEO flow that relies on electric field interaction with a charged EDL, electrothermal (*ET*) flow arises from the interaction of the external electric field with temperature-induced inhomogeneneities in medium conductivity and permittivity due to Joule heating.[7] Drawing on the fact that solution conductivity is weakly dependent on temperature, thermal gradients can generate conductivity gradients within a locally heated fluid space.

Current producing electrodes heat fluid locally to form a negative temperature gradient relative to the electrode surface. The resulting gradient induces a space charge accumulation and depletion under an AC field which similarly to ACEO flow, can interact with the applied field to generate a net body force on the liquid.[7] Space charge accumulation is a direct consequence of the temperature induced conductivity gradient; fluid nearest the surface is more conductive than the bulk resulting in a local discontinuity in electrical current, and accumulation of charge.

Unlike ACEO flow where the electric body force is limited to the thin EDL, temperature induced ET charging occurs over the length of the temperature gradient, typically tens of microns in thickness. Hence, ET micro-pumps can transport fluid past the electrode surface and the resulting ET induced fluid velocity is often an order of magnitude greater than conventional ACEO flow (100 μm s^{-1} *vs.* 1 mm s^{-1})[10]

ET micro-pumps are effective at fluid transport, however, they often require high media conductivity (>200 mS cm^{-1}) for adequate thermal effects, rendering them difficult to integrate with DEP. A typical cell's DEP response is strongly dependent on differences between cell interior and exterior buffer conductivities. Often high conductivity buffers such as those attributed with ET flow are similar in magnitude to a cell's interior and result in exceedingly weak (1 μm s^{-1}) DEP particle velocities.

ACEO flow is highly compatible with low conductivity buffers. Due to induced charging confined within the thin EDL, however, the resulting flow patterns are typically weak back pressure driven vortices. ET flow extends this region of charge outward by an order of magnitude to generate improved flow, but pumping is limited to high buffer conductive where DEP forces are often minute. For both strong pumping and cell DEP velocity we need a combination of these two effects – long range ET flow, but at a low buffer conductivity commonly associated with ACEO.

2.3 Electrothermal electro-osmosis

Recently, a new type of electrokinetic flow was observed.[10] As mentioned above, ACEO flow arises through charging of the thin EDL, while ET flow is generated *via* heat driven charge accumulation. We discuss combining both of these physical mechanisms for a more effective pump. In effect, localized heating is achieved within an extended EDL. The approach is to enlarge the double layer thickness, $\lambda_D = \left(\frac{\varepsilon D}{\sigma}\right)^{1/2}$, where are the medium dielectric constant, ion diffusivity and conductivity, respectively.[4] A low ionic strength high permittivity zwitterion buffer extends this characteristic length such that a thermal gradient exists in the double layer to enhance the charging rate. Strong *ET* flow can be generated with various types of low-conductivity and biologically compatible zwitterion buffers with low conductivities 100–160 μS cm^{-1}, two orders of magnitude less than what has been typically reported.[10]

Flow is generated with an asymmetrically polarized electrode array. As shown from a top view in Fig. 1A, one of the four electrodes is active, while the other three are grounded to produce a field focusing effect and a high thermal gradient emanating from the tip of the active electrode. Such asymmetry and the ET polarization mechanism discussed above lead to a net fluid motion down the length of the active electrode and a flow penetration depth of approximately 100 microns beyond the tip.

Based on experimentally measured velocity data, the observed fluid motion is not the typical ET flow, but rather an ET enhanced version of *AC* electro-osmostic flow – electrothermal electro-osmosis (ETEO). This phenomenon allow for high-velocity ETEO pumping at low electrolyte conductivities, as shown in Fig. 1B for the zwitterion buffer 6-aminohexanoic acid (AHA) under a range of applied voltages (15, 20, and 25V). A scaling analysis of the velocity data indicates that the characteristic double layer length scale specific to the electrolyte dielectric constant and conductivity needs to be included to demonstrate good data collapse of the measured fluid velocity.[10] These results suggest that the observed fluid motion is not the typical ET flow, but rather an ET enhanced version of ACEO flow, allowing high-velocity pumping at low DEP compatible buffer conductivities.

2.4 Dielectrophoresis for yeast cell separation

Dielectrophoresis, or DEP, commonly refers to the motion of a particle under the influence of a non-uniform electric field. For a homogenous spherical particle suspended in a media with a dielectric constant ε_m, classical theory models the induced particle DEP force, F_{DEP}, as[4,6]

$$F_{DEP} = 2\pi a^3 \varepsilon_m \mathrm{Re}(f_{cm}) \nabla |E|^2 \quad (1)$$

where a is the particle radius, E, the AC field strength and f_{cm}, the frequency depedent Clausius-Mossotti (*CM*) factor, $f_{cm} = (\varepsilon_p^* - \varepsilon_m^*)/(\varepsilon_p^* + 2\varepsilon_m^*)$. The complex permittivies of the particle, ε_p^*, and medium, ε_m^*, are each described by $\varepsilon^* = \varepsilon + \sigma/(i\omega)$, and model the charging of each frequency dependent domain as a lossy dielectric – a material that has both capacitive (dielectric charging) and resistive (conductive charging) elements.

At high frequencies when conductive charging does not have time to occur, differences in particle and media permittivity dominate the polarization at the particle interface. In contrast, low frequency polarization is governed by the disparity in conductivity, σ, between the two domains. A frequency characteristic of the inverse relaxation time (RC) separates these two distinct polarization mechanisms and is termed the DEP crossover frequency (*cof*). Depending on the sign of the interfacial charge, particles can be attracted or repelled from regions of high electric field intensity. The sign of this charge is captured in the *CM* factor.

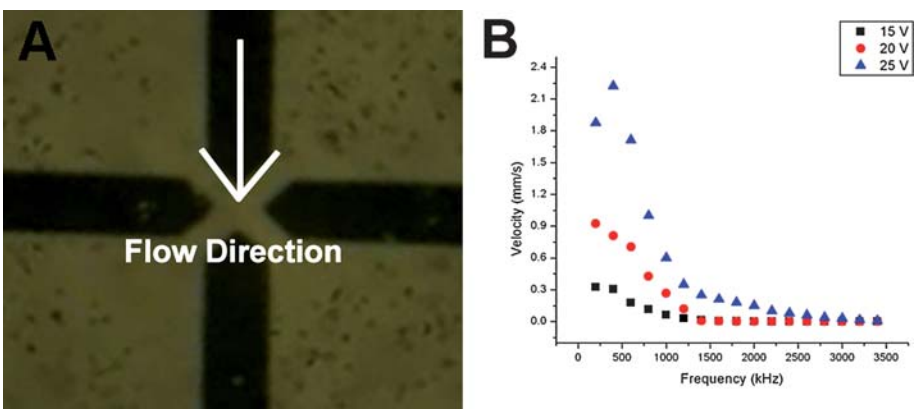

Fig. 1 (A) The fabricated micropump array. (B) Measured fluid velocity data for 1M AHA solution at 15V, 20V and 25 V, over a frequency range between 200 and 3200 kHz.

A positive real part to the *CM* factor indicates that the DEP force pushes a polarized particle towards a local electric field maximum, which is known as positive dielectrophoresis (pDEP), while a negative *CM* factor repels the particle away from the field maximum and towards regions of weak electric field, known as negative dielectrophoresis (nDEP). The frequency at which the *CM* factor equals zero is the *cof*. We measure the *cof* value by using a quadrupole electrode array. The array, as shown in Fig. 2 is symmetrically polarized such that every other electrode is active. This forms a low field region in the center of the array and a high field region at the edges of each of the four array electrodes. pDEP is observed when cells are attracted to the high field electrode edges (Fig. 2A) and nDEP is observed when the cells collect in the low field center of the array (Fig. 2B).

Cells, however, are more complex and exist as non-spherical particles with single or multiple shelled structures. As such, the classical DEP model must be modified. We use yeast as our model cell for DEP separation. A yeast cell is approximated as a dual-shelled oblate spheroid 7 μm in diameter, with a 5.8 μm domain of cytoplasm bound by a membrane of ~8 nm, shelled by a cell wall of ~200 nm, for a total of three interfaces,[21] as highlighted in Fig. 3.

Unlike homogenous particles with only one interface, the electric field is free to polarize a yeast cell at any of three interfaces: an inner cytoplasm-membrane, the membrane-cell wall, and an outer electrolyte-cell wall interface. As each domain has a different conductivity and dielectric constant each interface has a distinct relaxation timescale and frequency. A dual-shelled yeast cell therefore has the ability to exhibit two *cof's*: one a at low frequency (cof_1) governed by the relaxation time of the media/cell wall; and one at high frequency (cof_2) dependent on the relaxation time of the media/cytoplasm.

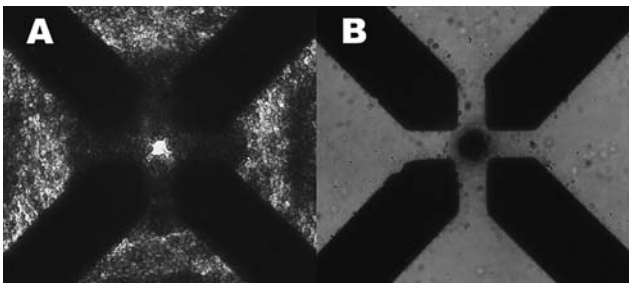

Fig. 2 Quadrupole electrode array used in *cof* measurements and preliminary DEP yeast cell study. (A) pDEP – cell attracted to high field electrode edges – of non-viable yeast. (B) Non-viable yeast attracted to low field electrode center (nDEP).

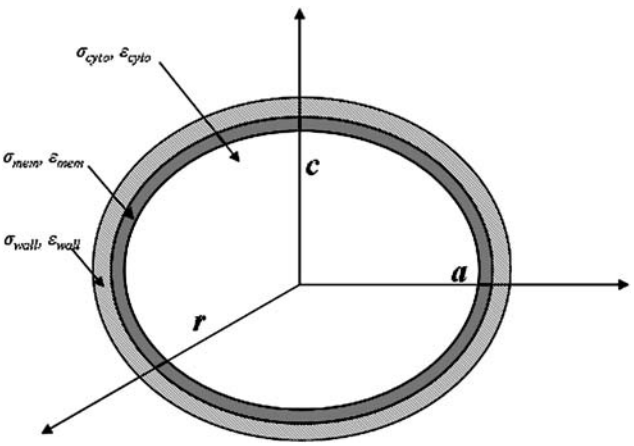

Fig. 3 Simplification of a dual shell-like structure of a yeast cell.

Based on the reported electric parameters for both viable and non-viable yeast cells the cell membrane is considered to be less conductive than the cell cytoplasm and cell wall.[21,22] Non-viable cells, however, are found to have a more conductive cell wall. As such, both low (100 kHz) and intermediate (~1 MHz) frequency regimes result in observed pDEP due to this more conductive cell wall. The cytoplasm dielectric constant, however, is still lower than the media and a high frequency AC field results in an observed nDEP behavior. Hence, non-viable yeast with a conductive cell wall exhibit one *cof* - determined by the inverse RC charging of the cytoplasm - and viable yeast cells with low cell wall conductivity display two.

As yeast cells are non-spherical and contain multiple interfacial domains, it is necessary to derive a modified *CM* factor to account for the cell wall, membrane, cytoplasm and non-spherical shape. The cell wall and membrane are modeled as thin shells surrounding an oblate spheroidal cytoplasm core, each with a specific complex permittivity. This system is modeled by deriving an effective complex permittivity for the entire three-domain system. First, the cytoplasm and surrounding membrane terms are replaced with a single effective complex term,[5,23]

$$\varepsilon'_{cyto-mem} = \varepsilon^*_{mem}\frac{\varepsilon^*_{mem} + \left(\varepsilon^*_{cyto} - \varepsilon^*_{mem}\right)\left[A_{ip} + v\left(1 - A_{op}\right)\right]}{\varepsilon^*_{mem} + \left(\varepsilon^*_{cyto} - \varepsilon^*_{mem}\right)\left[A_{ip} - vA_{op}\right]} \quad (2)$$

where ε_{mem}^* and ε_{int}^* are the complex permittivity of the cell membrane and interior, respectively. This process is repeated to include the permittivity of the cell wall (ε_{wall}^*), and yield the effective complex permittivity, ε'_{eff}, for the entire cell,

$$\varepsilon'_{eff} = \varepsilon^*_{m}\frac{\varepsilon^*_{wall} + \left(\varepsilon^*_{cyto-mem} - \varepsilon^*_{wall}\right)\left[A_{ip} + v\left(1 - A_{op}\right)\right]}{\varepsilon^*_{wall} + \left(\varepsilon^*_{cyto-mem} - \varepsilon^*_{wall}\right)\left[A_{ip} - vA_{op}\right]} \quad (3)$$

A_{op} describes the geometry-specific degree to which the exterior of the cell, extending from the outer membrane edge to infinity, depolarizes along the principal axis. For each of the two shells, A_{ip} describes the depolarization from just inside the membrane or cell wall to infinity. Other important parameters include $v = r^2c/[(r + d)^2(c + d)]$, the volume ratio of the cell exterior to interior, r, the cell radius, c, the cell half-length, and d, the cell membrane thickness. For a typical yeast cell, the cell membrane and cell wall are approximately 8 nm and 200 nm respectively, and at least an order of magnitude less than r and c; thus one can make the approximation $A_{op} = A_{ip}$. A useful expansion of this approximation can be expressed in terms of the scaling factor $\gamma = c/r$ as shown in (8.4):[5]

$$A_{op} = A_{ip} = \frac{\left[1 + \frac{3}{5}\left(1 - \gamma^{-2}\right) + \frac{3}{7}\left(1 - \gamma^{-2}\right)^2 + \ldots\right]}{3\gamma^{-2}} \quad (4)$$

For a sphere, $\gamma = 1$, and thus $A_{op} = A_{ip} = 1/3$, which forces this model to converge to the well-known *CM* factor for

a dual-shelled sphere. The yeast cells in this work have a measured scaling factor of approximately $c/r \sim 2.8\ \mu m/3.5\ \mu m \sim 0.8$. For the case of a dual-shelled oblate spheroid with major axis aligned parallel with the applied field, the *CM* factor can then be shown to be:[5]

$$f_{cm} = \frac{1}{3}\varepsilon_m \frac{\varepsilon'_{eff} - \varepsilon^*_m}{\left(\varepsilon'_{eff} - \varepsilon^*_m\right)A_{op} + \varepsilon^*_m} \quad (5)$$

From (5), a theoretical *cof* for viable and non-viable yeast can be calculated. Using reported electrical properties for viable and heat treated non-viable yeast cells[23] suspended in 1M 6-aminohexanoic acid (AHA) solution ($\sigma = 150\ \mu S\ cm^{-1}$, $\varepsilon = 160$) – a solution identical to that used in the above ETEO micro-pump - the modified *CM* factor for both viable and non-viable yeast has been calculated, as shown in Fig. 4.

As shown in the Figure, the DEP spectra of viable and non-viable yeast cells differ from one another. Non-viable cells due to their higher conductive cell wall have only one *cof*, while viable cells with a lower conducting wall have two. This plays an important and useful role in the design and utilization of DEP-based cell separation devices. Four DEP separation domains – **A**, **B**, **C** and **D** – have been highlighted in Fig. 4. Located far right at field frequencies less than ~100 kHz, domain **A** predicts that non-viable cells exhibit pDEP, while viable yeast and are repelled from high field regions under nDEP. Between 100 kHz–1.4 MHz (domain **B**), both viable and non-viable yeast suffer from pDEP. Hence, over this region both types of cells are attracted to the high field region. At frequencies between 1.4–2.2 MHz (domain **C**) the separation conditions reverse – non-viable cells display pDEP while viable exhibit nDEP. Finally, the opposite of domain B occurs at frequencies above 2.2 MHz – both cell types exhibit nDEP. These four DEP domains offer flexibility to the DEP researcher. Both non-viable and viable cells can be separately trapped in high field regions (pDEP), as indicated in domains **A** and **C**, respectively, and both cell types can be simultaneously trapped under either pDEP or nDEP within domains **B** and **C**, respectively. We will exploit these predicted domains for the development integrated cell separation devices.

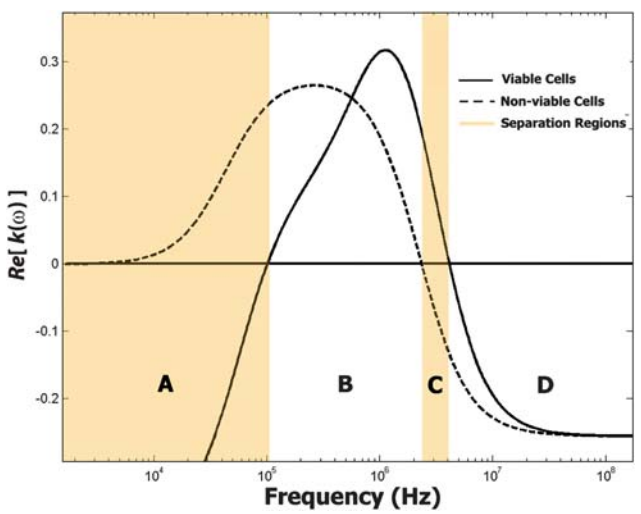

Fig. 4 The real part of the *CM* factor for both viable and non-viable yeast. Four domains of separation (A, C) and concentration (B, D) can be utilized due to differences in DEP mobility between these two cell types.

3.0 Electrokinetic integration

Experimental conditions for both DEP separation domains B and C are compatible with the conductivity range used in ETEO micro-pumping and integration of these two phenomena is possible. We combine these two phenomena within a PDMS microfluidic geometry. The objective is to use ETEO to circulate a cell suspension around a partially closed microfluidic loop to continually convect cells into the vicinity of a local DEP trap with every circulating pass. As such, DEP forces can be exerted on the cell suspension and eventually remove them from the flow field. Our goal is to feed the electrokinetic loop with a small syringe powered pressure driven flow. Different populations of cells enter the loop, electrokineticaly circulate, and are removed from the flow. We develop our basic microfluidic design below.

From the observed ETEO flow profile (Fig. 1A), the penetration length of the micro-pump – the length fluid can be pumped from and later penetrate off the electrode edge – is approximately 100 μm.[10] Over this active region the fluid velocity is on the order of ~500 μm s^{-1} while the measured DEP cell velocity is ~300 μm s^{-1} (both observed with an Olympus ISPEED high-speed camera at 10,000 fps). If the DEP trap is 50 μm in length and a cell is presumably moving with the flow field at a velocity of 500 μm s^{-1}, the cell will have 1/10 of a second to be removed from the flow field and trapped. Given the DEP cell velocity- which is different from the flow velocity - is ~300 μm s^{-1}, the cell be transported ~30 μm towards the DEP trap and cells 30 μm above the trap will fail to be removed from the flow field. One solution to this problem is to simply limit the micro-channel height to 30 μm. Taking into account the active pumping region and channel height limitations (<30 μm) microfluidic channel designs that take into account these two limits can be fabricated.

The first design is referred to as the square-loop design. Shown in Fig. 5A, the microelectrodes form a square pattern – each side 200 μm in length – with the active electrode regions in each corner of the device. The active electric field regions serve to both locally heat the electrolyte and to produce high electric field regions and both ETEO pumping and DEP trapping are accomplished with the same array of electrodes. A PDMS microchannel with a height of ~30 μm is fabricated by soft-lithography and sealed to the electrode substrate surface. This design serves as an ETEO induced circulating loop, whereby suspending cells are circulated around the loop and trapped at the high field regions located at the corners of the device.

The second generation device is a triangular loop (TL), shown in Fig. 5C. This design operates in a similar fashion as the square-loop. The triangular design eliminates one flow-restricting turn that fluid must overcome during transit. We utilize this device for DEP cell separation of non-viable cells (selectively stained blue) from viable cells. As will be discussed later in this article, we increase the channel height from the 30 μm channel used in the square loop to 55 μm to convert the system into a DEP cell separation device. Finally, the triangular loop has an additional DEP trap. This additional trap serves as a cell specific DEP valve to only allow a specific cell-subpopulation to exit the loop.

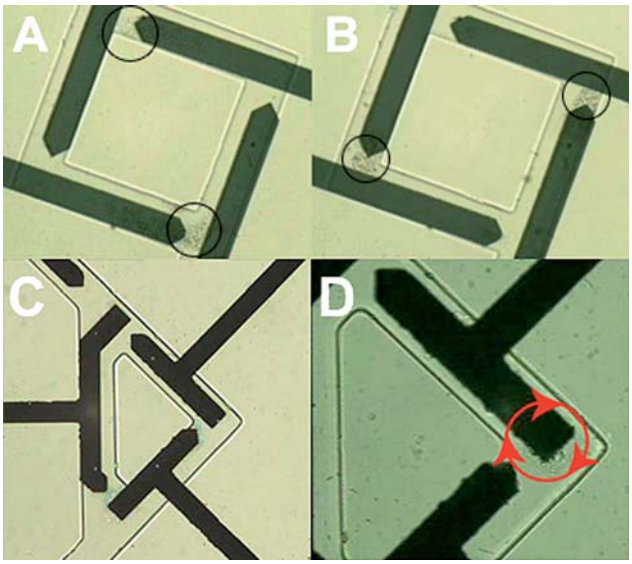

Fig. 5 (A–B) Fabricated microfluidic loop structures. (A) Square loop device that is used as a bulk cell trap. (B) Wiring configuration change results in cell trapping at different locations. (C–D) Triangular trap design for selective cell separation. (C) Separation of non-viable (blue) yeast from a 1 : 1 mixture of viable and non-viable yeast at a cell concentration of $\sim 10^6$ cells mL^{-1}. (D) Close-up of the DEP trap. Viable cells are separated from suspension and observed to rotate clockwise, indicated by the circular arrow direction.

4.0 Materials and methods

Electrode patterns were first fabricated by patterning dual titanium-gold layers onto pre-cleaned glass slides using standard lift-off techniques. Standard 50 × 75 mm pre-cleaned glass slides were patterned with the image reversal photoresist Shipley AZ-5214 to define the electrode patterns. Å of titanium and 2500 Å of gold were then evaporated onto the slides and the remaining resist was then removed in acetone. A 1M 6-amino-hexanoic acid (AHA) stock solution was prepared from reagent grade AHA obtained from Sigma-Aldrich. Conductivity measurements were measured with a conductivity probe and relative permittivity values were taken from literature.[24] Fluid velocity measurements (shown in Fig. 1B) were obtained by measuring the particle velocity of 5 μm polystyrene particles (Polyscience) using a high speed camera (Olympus ISPEED) at 10,000 fps attached to an inverted microscope (Olympus IX71). DEP velocity measurements were performed by measuring particle velocity in the absence of fluid flow over a symmetrically polarized electrode array. As field focusing and the resulting ETEO flow was eliminated, DEP velocity was isolated and measured. The AHA solution was injected into a cover slip sealed array and fluid velocity was measured between 200–1200 kHz at 15, 20, and 25 V_{pp} over the tip of the active electrode for the asymmetrically polarized array. The wiring configuration was modified and the DEP velocity measurements were then performed.

After the electrodes were fabricated and characterized, microchannels were fabricated using well-known soft-lithography techniques.[25] A 10 : 1 ratio of elastomeric base and curing agent (Sylgard 184 – Dow Corning) was mixed and poured atop the thick SU-8 patterned glass slide and baked for 1 h at 65 °C. Following photoresist curing the thickness of the mold was measured (Alpha Step 500) to determine the microchannel height. During this time the elastomeric base conforms to the SU-8 mold, cures, and hardens into a flexible polymeric slab. The slab was then gently peeled off the slide. Holes were then punched into the PDMS to serve as the channel fluid inlet and outlet using a biopsy punch (0.75 mm, Ted-Pella, Inc., Redding CA).

The final and most delicate fabrication step involves aligning the PDMS polymer slab atop the appropriate microelectrode geometry, oxidizing both surfaces while under alignment, and finally bringing them into conformal contact and creating an irreversible bond at the PDMS-glass interface. Because oxidation of each surface – PDMS and glass – is highly unstable and reversible in an oxygen environment – lasting no more than 3 min – it is important to have the sample properly aligned prior to oxidation so that the strongest possible seal is made. This is done by employing a custom-made micromanipulator to align the PDMS slab with the fabricated microelectrodes. Once aligned both are subjected to an oxygen plasma to activate the glass and polymer surfaces, so when placed in conformal contact they irreversibly bond to each other.[25] The micromanipulator design is comprised of two 200 micron-thick glass cover slips reversibly attached to the bottom edges of the PDMS slab. The cover slips facilitate alignment – one can simply 'glide' the PDMS molded microchannels across the microelectrode patterned glass slide. The 200 micron gap formed by the cover slips allows alignment of both the microchannel and electrode structures while under a microscope (Olympus IX71); the gap also permits each surface to be exposed to oxygen plasma and oxidized. Utilizing this 'glide' technique, the two patterns are aligned by hand, the cover slips are gently taped down with Scotch tape, and the entire device is placed in an oxygen plasma oven (Drytek plasma etcher) and exposed to oxygen plasma for 1 min at 1400 mW. The PDMS slab is then immediately brought into conformal contact with the glass slide and firmly held in place for 30 s, after which the cover slips are gently peeled from the edges of the PDMS. This results in an irreversible permanent bond between the aligned PDMS and glass surface.[25]

After the device is fabricated, the yeast cell culture was prepared. 5 grams dry weight of commercial grade bakers yeast (*Saccharomyces cerevisiae*) was dissolved in 50 mL of culture medium, pH 5, consisting of 5 g l^{-1} yeast extract, 5 g l^{-1} bacterial peptone and 50 g l^{-1} sucrose. The yeast was grown at 37 °C for 36 h and four 1 mL samples were harvested, each washed 4 times in 280 mM mannitol. Two samples were rendered non-viable by heating at 90 °C. Non viable cell samples are washed as before and all four samples stained with 80 μL of methylene blue (Sigma-Aldrich), as described in other studies.[26,27] Non-viable cells are washed 3 times in 280 mM mannitol and all four samples are then suspended in 1M AHA solution.

DEP *cof* measurements are made using a quadrupole electrode array. The array electrodes are patterned using identical fabrication procedures as described above. The fabricated array, as shown in Fig. 2(A–B), was attached to a function generator set to 10 Vpp (Agilent, model #33220A) *via* copper tape and symmetrically activated by polarizing every other electrode. Structurally, the array is identical to the ETEO pump (Fig. 1A), however, the symmetric wiring arrangement creates a field minimum in the center region of the four electrodes and field

maxima along the electrode edges. The array is covered with a plastic cover slip and injected with yeast cell suspension. The field frequency is slowly increased from 1 kHz to 20 MHz in order to determine yeast cell *cof* and DEP velocity. The suspension *cof* was taken when the cells migrated from the electrode edges (Fig. 2A) to the electrode center (Fig. 2B).

Once the *cof* is known, PE20 tubing is inserted into the PDMS biopsy punched ports of the microfluidic device and the cell solution is transported into the microchannel using a syringe pump. Frequency controlled voltage signals are then delivered to the electrodes using a function generator (Agilent, model #33220A).

5.0 Results and discussion

5.1 DEP analysis of viable and non-viable yeast

Using the quadrupole electrode array shown in Fig. 2(A–B), we studied the DEP *cof* of both viable and non-viable yeast suspended in 1M AHA solution to determine optimal conditions for DEP-induced cell separation. Viable yeast cells show two *cof* values – one at 75 kHz and a second *cof* at 2.6 MHz. Unlike viable yeast, non-viable cells with a more conductive cell wall reveal only one *cof* at 2.2 MHz. As such, the *cof* spectrum as predicted in Fig. 4 agrees well with measured cof values.

One can separate non-viable yeast from viable over two unique frequency ranges, earlier termed domain A and C. Shown in Fig. 4 as domain A, frequencies below 110 kHz non-viable (stained blue) yeast become repelled from high field regions and separate from viable yeast. Increasing frequency between 150 kHz–2.2 MHz both viable and non-viable cells suffer pDEP. As such, separation is not possible over this frequency range (domain B), only bulk concentration. The second separation range occurs over domain C between 2.2 and 2.6 MHz and is limited by the second crossover of viable yeast. Contrary to domain A, non-viable cells migrate into field minimum (nDEP) and viable cells separate out of suspension *via* pDEP. Increasing frequency above 2.6 MHz forces both cell types to collect in the quadrupole's low field region, and bulk nDEP concentration occurs. The fact that viable cells have two *cof* values and non-viable cells have only can therefore produce four useful DEP manipulation schemes: pDEP separation of viable yeast (A), pDEP concentration of a viable and non-viable yeast (B), pDEP separation of non-viable yeast (C), and nDEP concentration of a viable and non-viable yeast (D).

We experimentally observed all four DEP domains – A, B, C, and D – with a 1 : 1 mixture of viable and non-viable cells and show the results in Fig. 6(A–D), with each lettered Figure section relating to a DEP domain (Fig. 4). We must note that the separation was not entirely efficient, as small amounts of viable cells appeared to irreversibly adhere to the electrode edges and failed to repel from this region throughout the entire experimental frequency range. This is apparent in Fig. 6D, where one can observe a small number of viable cells on the high field electrode edge region.

5.2 Integrated electrokinetic separation

We now test our integrated on-chip electrokinetic separation strategy both with active DEP traps and ETEO pumps. We first test the square loop design described earlier in this work. The device, shown in Fig. 5A, consists of a square fluidic loop connected to an inlet and outlet channel. The key feature of this design is that the DEP trapping zones can be relocated by changing the location of the active electrodes. If we imagine splitting the four sides of a square into two adjacent triangles and apply an identical in phase AC voltage to the left-side pair, no electric field will exist over the pair gap. Similarly, by grounding the right-side pair, the effect is the same; there is no electric field between the pair gap. This is not the case, however, across the electrode gaps between the electrode pairs. Due to a voltage drop across these two pair forming gaps, there exists two high field regions spaced on opposing corners of the square device, as indicted by the two circled corners in Fig. 5A. If we rotate the location of the active AC voltage in a counter-clockwise direction the location of the active electric field regions also shift counter-clockwise, as indicated by the two circled corners in Fig. 5B. Hence, we can change the active trapping and pumping locations within the square loop by a simple rotation of the electrode wiring. The pumping direction (counter-clockwise), however, remains the same. For this particular electrode geometry the flow direction is always in the counter-clockwise direction. As the high field polarized electrode tips point in the counter-clockwise direction the fluid becomes locally heated and pumped *via* ETEO in the direction of the active pumping zones on each electrode.

We now test this concept. A 1 : 1 mixture of viable:non-viable yeast was pumped slowly through the device at a flowrate of 0.5 μL h^{-1}, with an applied voltage and frequency of 25 V_{RMS} and 75 kHz, respectively. The device was wired such that the circled field regions in Fig. 5B were active. The fluid immediately started to circulate counter clockwise around the square loop with fluid velocity of ~ 290 μm s^{-1} (measured at 10 000 fps). Cells circulated with the moving fluid and over a period of 10 s concentrated at both active field corners of the loop (Fig. 5A).

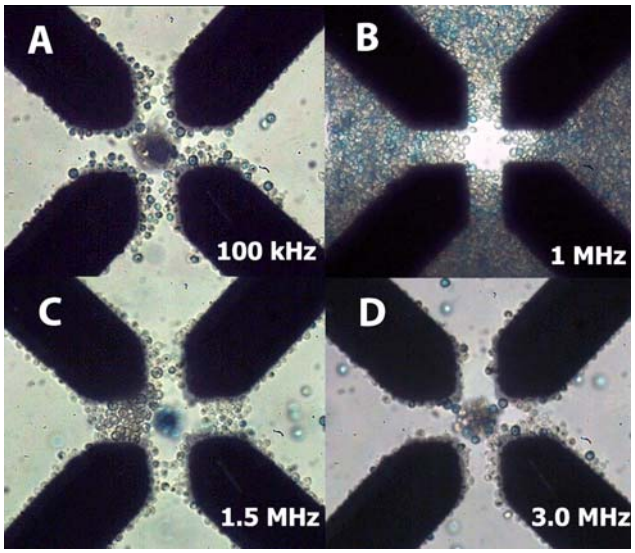

Fig. 6 Four distinct DEP domains of viable:non-viable cell mixtures. (A) pDEP separation of non-viable (blue) cells. (B) pDEP concentration of both cell types (C) pDEP separation of viable cells. (D) nDEP concentration of both cell types.

This residence time translates into about 4 circuits around the loop and visits to 16 trapping stations.

We then deactivated the device and rotated the wiring counter-clockwise, relocating the high field to the circled regions in Fig. 5B. The device was activated and the cells were immediately released from the previous high field regions to the newly active regions. Both cell types, however, quickly collected over the active field regions during both of our experiments. From a pure dielectrophoretic argument, this result is unexpected. In both cases, the 75 kHz frequency should lead to non-viable cell attraction and viable cell repulsion, and ultimately cell separation. This was not observed, as both cell types were seemingly attracted to the high field region.

As mentioned earlier in this work, the channel height of the device was 30 μm. This is similar in length to each side pair's electrode gap (25 μm), which is of the order of the field penetration length – the distance the field can penetrate into the microchannel. It follows that if the electric field can penetrate into the entire cross-section of the microchannel, perhaps those cells affected by nDEP run into a virtual pDEP "wall" driven by the electric field and repel from this field induced blockage, continually driven into it by the resulting ETEO flow. The solution to this problem can be met by increasing the drag force on the cell and hence increase the force in which it is driven into the "wall" and eventually overcome the pDEP trap. Alternatively, one can decrease the field penetration length relative to the channel height to create a low-field region within the upper regions of the flow profile. As such, nDEP affected cells would no longer hit the pDEP "wall" and be allowed to pass. Based on this, we describe an alternative design to the square-loop, one that operates with both an increase fluid velocity and channel height.

As opposed to simply increasing both the channel height and applied voltage – and hence the ETEO velocity – of the square loop design, we take a different approach with a new loop design. Our second generation design is essentially the square loop sliced diagonally in half, forming a triangular loop with similarly connected inlet and outlet ports, as shown in Fig. 5C. The triangular design removes one corner, and hence one sharp turn, that the fluid must overcome during circulation. As such, back pressure losses associated with two-dimensional fluid boundary layer separation are immediately reduced by 25%. We believe these fluid back pressure losses to play a significant role in determining the critical circulating velocity of the device.

It is well known that boundary layer separation due to a sudden drop of imparted momentum in the new flow direction can produce a circulating eddy near a sharp turn.[28] Similarly, we also observe circulating vortices over the active high-field regions of our device which we believe are driven by such boundary layer detachment. In fact cells are observed to rapidly circulate within the confined region of the DEP trap during device operation. Hence, the removal of one corner of the loop should lead to an increase in observed flow velocity over the original square loop design. We believe this, combined with an increase in channel height is what leads to the improved cell separation performance over the square loop.

The triangular loop was wired similarly to the square design. Again, every other electrode in the triangle was active, such that now only two trapping zones exist. The device was activated under identical conditions as the square loop – 25 V_{RMS} and 75 kHz – and the resulting circulation velocity was observed to be $\sim$330 μm s^{-1} – a 14% increase over the square design. To account for the increase in flow, an additional electrode with a larger 80 μm separation and high field penetration length was added at the device exit to aid in preventing unwanted cell removal from the increased circulating flow rate. The electrode was independently controlled to act as a particle valve; fluid was free to exit the device while cells were either trapped at the high field region (pDEP) or forced into the valve's "wall" where they soon were observed to be swept back into circulation.

We tested the triangular loop on a mixture of 5% non-viable, 95% viable yeast cells at a cell concentration of $\sim 10^6$ cells mL^{-1}. Non-viable cells, as mentioned earlier, were selectively stained blue. Similarly to the square loop, fluid entered the device at a flow rate of 0.5 μL h^{-1} and an applied voltage and frequency of 25 V_{RMS} and 75 kHz, respectively (domain A). A second experiment was performed aimed at trapping viable yeast *via* pDEP (domain C). In this particular experiment, fluid entered the device at an identical flow rate (0.5 μL h^{-1}) and applied voltage (25 V_{RMS}), but now driven instead by a high frequency (2.3 MHz) signal. The DEP "valve" was activated at a frequency of 200 kHz – a frequency known to both force non-viable cells away from the fluid exit stream and to concentrate viable cells *via* pDEP. As such, the additional DEP trap served as a selective particle filter within the loop, diluting viable cells from circulation while at the same time increasing non-viable cell residence time.

We first tested the triangular loop within domain A (75 kHz). After approximately 2 min of operation faint blue patches of cells were observed on the active trapping zones, shown in Fig. 5C. This translates into more than 150 loops around the triangular circuit or nearly 500 DEP trap stations visited. A linear channel that offers as many visits would be more than 12 cm long. The second high frequency experiment at 2.3 MHz (domain C) was performed. As viable cells are somewhat transparent and difficult to observe, a higher magnification image of the viable yeast cell trap is shown in Fig. 5D. In both we observed cell rotation at the corner traps, as described by the circular arrowed pattern in Fig. 5D. This leads us to believe that sharp-corner back pressure plays a role in limiting the critical flow velocity in our circulating devices. When, the triangle design was implemented with high fluid velocity and a larger channel height. This allowed nDEP induced cells to bypass the high field region, continue circulating and eventually exit the flow loop, enabling selective cell separation.

6.0 Conclusions

Based on this work, we believe that ETEO and DEP can be integrated into polymer microchannels to produce cell processing units that include circulating loops – a design that is difficult to produce with other microfluidic technologies. By understanding the frequency and buffer dependence for both ETEO fluid flow and DEP induced cell behavior, and by integrating these phenomena into insulating PDMS microchannels, a wide array of cellular manipulation options becomes possible. We have demonstrated the ability to selectively trap and concentrate viable, non-viable, and both cell types simultaneously at specific pDEP and nDEP traps. The next step in development should

involve connecting a large array of the mm-sized loops into a massive array, with possible fluid/particle transport from one loop unit to all neighboring units – upstream, downstream and parallel connectivity is now possible. In this way, specific cell types can be extracted and trapped in one loop, while the remaining cells continue to flow through to be later sorted in other downstream loops. This would allow for more complex cell processing. For example, if both cell concentration and separation was required on one device, circulating loops of different channel height could be connected in series and used together. Such flexibility could produce a new dimension in the ever-expanding universe of microfluidic technologies.

References

1 C. H. Chen and J. G. Santiago, A planar electroosmotic micropump, *J. Micromech. Microeng*, 2002, **11**, 672–683.
2 A. Gonzalez, N. G. Green, A. Castellanos and H. Morgan, Fluid Flow induced by nonuniform ac electric fields in electrolyes on microelectrodes II. A linear double-layer analysis, *Phys. Rev. E: Stat. Phys., Plasmas, Fluids, Relat. Interdiscip. Top.*, 2000, **61**, 4019–4028.
3 A. Ramos, H. Morgan, N. G. Green and A. Castellanos, AC electrokinetics: a review of forces in microelectrode structures, *J. Phys. D: Appl. Phys.*, 1998, **31**, 2338–2353.
4 H. Morgan, N. Green, *AC Electrokinetics: Colloids and Nanoparticles*, Research Studies Press, Hertfordshire, England, 2003.
5 T. B. Jones, *Electromechanics of Particles*, Cambridge University Press, Cambridge, 1995.
6 N. G. Green and H. Morgan, Dielectrophoretic separation of nanoparticles, *J. Phys. D: Appl. Phys.*, 1997, **30**, L41–L44.
7 J. Wu, M. Lian and K. Yang, Micropumping of biofluids by alternating current electrothermal effects, *Appl. Phys. Lett.*, 2007, **90**, 234103.
8 N. G. Green, A. Ramos, A. Gonzalez, H. Morgan and A. Castellanos, Fluid flow induced by nonuniform ac electric fields in electrolytes on microelectrodes. I. Experimental measurements, *Phys. Rev. E: Stat. Phys., Plasmas, Fluids, Relat. Interdiscip. Top.*, 2000, **61**, 4011–4018.
9 A. Ramos, A. Gonzalez, A. Castellanos, N. G. Green and H. Morgan, Pumping of liquids with ac voltages applied to asymmetric pairs of electrodes, *Phys. Rev. E*, 2003, **67**, 056302-1–056302-11.
10 Z. R. Gagnon and H. Chang, Electrothermal ac electro-osmosis, *Appl. Phys. Lett.*, 2009, **94**, 024101–024101.
11 D. Lastochkin, R. Zhou, P. Wang, Y. Ben and H.-C. Chang, Electrokinetic micropump and micromixer design based on ac faradaic polarization, *J. Appl. Phys.*, 2004, **96**, 1730–1733.
12 G. Markx, M. Talary and R. Pethig, Separation of viable and non-viable yeast using dielectrophoresis, *J. Biotechnol.*, 1994, **32**, 29–37.
13 W. Arnold, Positioning and levitation media for the separation of biological cells, *IEEE Trans. Ind. Appl.*, 2001, **37**, 1468–1475.
14 J. Kadaksham, P. Singh and N. Aubry, Dielectrophoresis induced clustering regimes of viable yeast cells, *Electrophoresis*, 2005, **26**, 3738–3744.
15 J. Crane and H. Pohl, A study of living and dead yeast cells using dielectrophoresis, *J. Electrochem. Soc.*, 1968, **115**, 584–586.
16 T. Christensen, C. Pedersen, D. Bang and A. Wolff, Sample preparation by cell guiding using negative dielectrophoresis, *Microelectron. Eng.*, 2007, **84**, 1690–1693.
17 C. Kua, Y. Lam, I. Rodriguez, C. Yang and K. Youcef-Toumi, Dynamic cell fractionation and transportation using moving dielectrophoresis, *Anal. Chem.*, 2007, **79**, 6975–6987.
18 N. Demierre, T. Braschler, R. Muller and P. Renaud, Focusing and continuous separation of cells in a microfluidic device using lateral dielectrophoresis, *Sens. Actuators, B*, 2008, **132**, 388–396.
19 T. Braschler, N. Demierre, E. Nascimento, T. Silva, A. Oliva and P. Renaud, Continuous separation of cells by balanced dielectrophoretic forces at multiple frequencies, *Lab Chip*, 2008, **8**, 280–286.
20 T. Thorsen, S. J. Maerkl and S. R. Quake, Microfluidic large-scale integration, *Science*, 2002, **298**, 580–584.
21 R. Holzel and I. Lamprecht, Dielectric properties of yeast cells as determined by electrorotation, *Biochim. Biophys. Acta, Biomembr.*, 1992, **1104**, 195–200.
22 Y. Huang, R. Holzel, R. Pethig and X. Wang, Differences in the ac dynamics of viable and non-viable yeast cells determined through combined dielectrophoresis and electrorotation studies, *Phys. Med. Biol.*, 1992, **37**, 1499–1517.
23 M. P. Hughes, *Nanoelectromechanics in Engineering and Biology*, CRC Press, Boca Raton, Florida, 2003.
24 W. M. Arnold and U. Zimmermann, Dielectric Properties of Zwitterion Solutions, *Biochem. Soc. Trans.*, 1993, **21**, 475S.
25 Y. Xia and G. Whitesides, Soft Lithography, *Annu. Rev. Mater. Sci.*, 1998, **28**, 153–184.
26 J. E. Gordon, Z. Gagnon and H.-C. Chang, Dielectrophoretic discrimination of bovine red blood cell starvation cage by buffer selection and membrane cross-linking, *Biomicrofluidics*, 2007, **1**, 044102(1–5).
27 Z. Gagnon, J. Mazur and H.-C. Chang, Glutaraldehdye enhanced dielectropnoretic yeast cell separation, *Biomicrofluidics*, 2009, **3**, 044108(1–11).
28 W. Deen, *Analysis of Transport Phenomena*, Oxford University Press, 1998.

